carcinoma: a morphometric study. *Hum Pathol* 1992; **23**: 619–26.
10 Honda H, Tajima T, Kajiyama K *et al.* Vascular changes in hepatocellular carcinoma: correlation of radiologic and pathologic findings. *AJR Am J Roentgenol* 1999; **173**: 1213–7.
11 Higashihara H, Okazaki M. Transcatheter arterial chemoembolization of hepatocellular carcinoma: a Japanese experience. *Hepatogastroenterology* 2002; **49**: 72–8.
12 Nakao N, Miura K, Takahashi H *et al.* Hepatocellular carcinoma: combined hepatic, arterial, and portal venous embolization. *Radiology* 1986; **161**: 303–7.
13 Yamakado K, Hirano T, Kato N *et al.* Hepatocellular carcinoma: treatment with a combination of transcatheter arterial chemoembolization and transportal ethanol injection. *Radiology* 1994; **193**: 75–80.
14 Miyayama S, Matsui O, Yamashiro M *et al.* Ultraselective transcatheter arterial chemoembolization with a 2-F tip microcatheter for small hepatocellular carcinomas: relationship between local tumor recurrence and visualization of the portal vein with iodized oil. *J Vasc Interv Radiol* 2007; **18**: 365–76.
15 Miyayama S, Mitsui T, Zen Y *et al.* Histopathological findings after ultraselective transcatheter arterial chemoembolization for hepatocellular carcinoma. *Hepatol Res* 2009; **39**: 374–81.
16 Iwamoto S, Yamaguchi T, Hongo O, Iwamoto H, Sanefuji H. Excellent outcomes with angiographic subsegmentectomy in the treatment of typical hepatocellular carcinoma: a retrospective study of local recurrence and long-term survival rates in 120 patients with hepatocellular carcinoma. *Cancer* 2010; **116**: 393–9.
17 Kim HC, Chung JW, Lee W, Jae HJ, Park JH. Recognizing extrahepatic collateral vessels that supply hepatocellular carcinoma to avoid complications of transcatheter arterial chemoembolization. *Radiographics* 2005; **25**: S25–S39.
18 Miyayama S, Matsui O, Taki K *et al.* Extrahepatic blood supply to hepatocellular carcinoma: angiographic demonstration and transcatheter arterial chemoembolization. *Cardiovasc Intervent Radiol* 2006; **29**: 39–48.
19 Ueda K, Matsui O, Kawamori Y *et al.* Hypervascular hepatocellular carcinoma: evaluation of hemodynamics with dynamic CT during hepatic arteriography. *Radiology* 1998; **206**: 161–6.
20 Tochio H, Tomita S, Kudo M *et al.* [The draining vessels of advanced hepatocellular carcinoma: assessment of color Doppler findings in comparison with histopathological findings.] *Acta Hepatol Jpn* 1999; **40**: 243–52. (In Japanese.)
21 Ueda K, Saito K, Terada T, Nakanuma Y. Selective necrosis of encapsulated malignant lesion with atypical adenomatosu hyperplasia of the liver following transarterial embolization. A report of two autopsy cases. *J Clin Gastroenterol* 1991; **13**: 709–14.
22 Miyayama S, Matsui O, Yamashiro M *et al.* Iodized oil accumulation in the hypovascular tumor portion of early-stage hepatocellular carcinoma after ultraselective transcatheter arterial chemoembolization. *Hepatol Int* 2007; **1**: 451–9.
23 Liu Y, Matsui O. Changes of intratumoral microvsessels and blood perfusion during establishment of hepatic metastases in mice. *Radiology* 2007; **243**: 386–95.
24 Kitao A, Zen Y, Matsui O, Gabata T, Nakamura Y. Hepatocarcinogenesis: multistep changes of drainage vessels at CT during arterioportography and hepatic arteriography – Radiologic-pathologic correlation. *Radiology* 2009; **252**: 605–14.
25 Kudo M. Atypical large well-differentiated hepatocellular carcinoma with benign nature: a new clinical entity. *Interviology* 2004; **47**: 227–37.
26 Hirano K, Kondo Y, Teratani T *et al.* Hepatocellular carcinoma depicted as hypoattenuation on CT hepatic arteriography (CTA) and hyperattenuation on CT during arterial portography (CTAP). *J Gastroenterol* 2001; **36**: 346–9.

Jpn J Radiol (2011) 29:371–377
DOI 10.1007/s11604-011-0568-8

PICTORIAL ESSAY

Efficacy of cone-beam computed tomography during transcatheter arterial chemoembolization for hepatocellular carcinoma

**Shiro Miyayama · Masashi Yamashiro · Yuki Hattori
Nobuaki Orito · Ken Matsui · Kazunobu Tsuji
Miki Yoshida · Osamu Matsui**

Received: October 12, 2010 / Accepted: January 20, 2011

Abstract Cone-beam computed tomography (CBCT) using a flat-panel detector is an alternative method of obtaining cross-sectional images. This technique is now being used during transcatheter arterial chemoembolization (TACE) for inoperable hepatocellular carcinoma (HCC). Several CBCT techniques are performed to detect HCC lesions: CBCT during portography (CBCTAP), CBCT during hepatic arteriography (CBCTHA), CBCT after iodized oil injection (LipCBCT), CBCT during arteriography (CBCTA) of extrahepatic collaterals. Almost all HCC lesions can be detected using these CBCT images. Three-dimensional arteriography using maximum intensity projection from CBCTHA images can identify the tumor-feeding branch. In particular, this technique is useful when the tumor stain cannot be demonstrated on arteriography. In addition, dual-phase CBCTHA can improve the diagnostic accuracy for hypervascular HCCs because corona enhancement can be detected around the tumor. To monitor the embolized area during TACE, selective CBCTHA or LipCBCT at the embolization point is useful. Two sequential CBCT scans without and with contrast material injection is also useful to confirm each embolized area of two vessels. Furthermore, CBCTA can prevent nontarget embolization. Although the image quality of CBCT is low compared to that of conventional CT, CBCT provides useful information that helps perform TACE for HCCs safely and effectively.

Key words Cone-beam computed tomography · Hepatocellular carcinoma · Transcatheter arterial chemoembolization

S. Miyayama (✉) · M. Yamashiro · Y. Hattori · N. Orito · K. Matsui · K. Tsuji · M. Yoshida
Department of Diagnostic Radiology, Fukuiken Saiseikai Hospital, 7-1 Funabashi, Wadanaka-cho, Fukui 918-8503, Japan
Tel. +81-776-23-1111; Fax +81-776-28-8519
e-mail: s-miyayama@fukui.saiseikai.or.jp

O. Matsui
Department of Radiology, Kanazawa University Graduate School of Medical Science, Kanazawa, Japan

Introduction

Transcatheter arterial chemoembolization (TACE) is one of the effective treatments for inoperable hepatocellular carcinoma (HCC). During the TACE procedure, computed tomography (CT)—during arterial portography (CTAP) and during hepatic arteriography (CTHA)—is helpful for identifying hypervascular HCC lesions for treatment.

To perform TACE effectively, superselective catheterization is essential not only through hepatic branches but also through extrahepatic collaterals. However, small tumor-feeding branches may be missed when the catheter is advanced too far into the tumor-feeding branches.[1] In addition, complications may develop when nontumor-feeding extrahepatic branches are inadvertently embolized.[2–5] Intraprocedural monitoring of the embolized area is necessary to improve local control while reducing adverse effects of TACE.[6]

Cone-beam CT (CBCT) technology using a flat-panel detector (FPD) is an alternative method of obtaining cross-sectional images. This technique is currently being combined with TACE for HCC.[7–12] In this article, we describe the efficacy of CBCT during TACE for HCC.

CBCT technique

An angiographic unit with an FPD can obtain CBCT images. In our CBCT protocol (XperCT; Philips Medical Systems, Best, the Netherlands), 321 projection images with X-ray parameters of 120 kV and 50–325 mA are obtained by 10.4-s acquisition with 207° rotation of a 30 × 38 cm FPD of the angiographic C-arm around the patient. CBCT can be obtained simply by lifting the patients' hands, without other movement. The maximum radiation dose of a single CBCT measured on a CT phantom is 22.3 mGy. Since August 2009, we have used a prototype of the dual-phase CBCT software (Philips Medical Systems). The first phase is scanned during a clockwise rotation and the second phase during a counterclockwise rotation. The minimum interval between the end of the first scan and the start of the second scan is 4 s.

Optimal thick cross-sectional images are obtained for observation of CBCT images on a workstation (Philips Medical Systems). The matrix size is 512 × 512, and the field of view (FOV) is 25 cm. Maximum intensity projection (MIP) images from CBCT can also be used to observe the vascular anatomy.

Detection of HCC by CBCT

Several CBCT techniques are performed during the TACE procedure: during arterial portography (CBCTAP), during hepatic arteriography (CBCTHA), and after iodized oil (Lipiodol; Andre Guerbet, Aulnay-sous-Bois, France) injection (LipCBCT). All three techniques correspond to CTAP, CTHA, and Lipiodol-CT obtained by a conventional CT scanner. During CBCTAP, 40 ml of contrast material [370 mg I iopamidol (Iopamiron 370); Bayer, Osaka, Japan] is injected at a rate of 3 ml/s through a 4F catheter placed into the superior mesenteric artery after administration of 2.5 μg of prostaglandin E_1 (PGE_1) (Liple; Tanabe Mitsubishi, Osaka, Japan). When the replaced hepatic branches or arterial flow toward the liver from the superior mesenteric artery is demonstrated, the catheter tip is deeply advanced avoiding these branches. Scanning begins 25 s after the start of the contrast material injection. CBCTHA is performed during the common or proper hepatic, right or left hepatic, or selective arteriography of the liver. When CBCTHA is performed at the common or proper hepatic artery, 25–40 ml of half-diluted contrast material is injected at a rate of 1.5–2.0 ml/s through a 4F catheter. When CBCTHA is performed at a more distal level of the right or left hepatic artery (selective CBCTHA), 5–10 ml of half-diluted contrast material is slowly injected manually through a microcatheter. Scanning starts 7 s after the beginning of the contrast material injection. LipCBCT is also performed after injection of a mixture of 1–3 ml of iodized oil and anticancer drugs. This technique is mainly performed when blood supply to the tumor from the selected branch is highly suspected or when iodized oil accumulation in the tumor is unclear during TACE despite tumor feeding on selective CBCTHA images. In addition, this technique is performed when the selected branch is minute, and contrast material easily overflows despite careful hand injection. CBCT during arteriography (CBCTA) of extrahepatic collaterals is also performed to confirm an extrahepatic blood supply to an HCC using 5–10 ml of half-diluted contrast material.

In a previous report, 89% of HCC nodules (mean diameter ± standard deviation, 1.9 ± 1.1 cm) could be detected by CBCTAP compared to conventional CTAP.[9] In addition, all small HCCs (mean diameter 1.3 ± 0.3 cm) that could not be detected on arteriography could be depicted by combined with CBCTAP, CBCTHA, and LipCBCT (Figs. 1–11).[10] Among these images, LipCBCT is the most sensitive for detecting small HCC nodules because of the high contrast of iodized oil (Fig. 2).[10]

Detection of corona enhancement around HCC

Corona enhancement represents venous drainage through hypervascular HCC nodules.[13,14] It is one of the most reliable findings for distinguishing between HCCs and arterioportal shunts.[15] In a previous report, corona enhancement was detected in 89% of HCC lesions. It had a mean diameter of 1.8 ± 0.9 cm on second-phase CBCTHA images obtained 30 s after the end of the first scan (Figs. 3, 4; see also Fig. 11, below), although it could not be detected around small tumors.[12] In contrast, corona enhancement is not seen around hypervascular pseudolesions, such as arterioportal shunts (Fig. 4).[12,15] This technique can improve the diagnostic accuracy of hypervascular HCC nodules by CBCTHA. In addition, the area of corona enhancement should be included to the safety margin of the treatment because HCC cells spread mainly via the drainage route. Therefore, depiction of corona enhancement on CBCTHA is meaningful when determining the adequacy of the embolized area during TACE.

Identification of tumor-feeding branch

Slab-MIP images from CBCTHA can identify not only the tumor stain but also the tumor-feeding branch.[11] These images are particularly useful when a tumor stain is unclear on arteriography. Observation of slab-MIP images at the optional thickness and direction using a

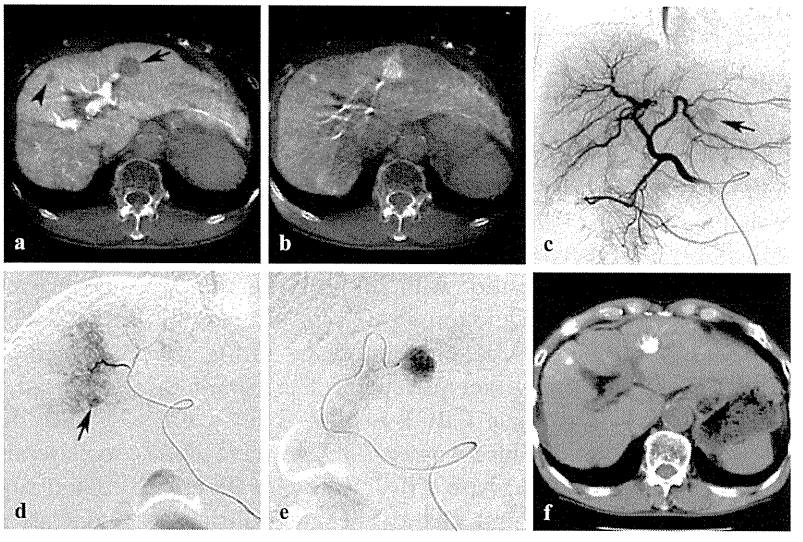

Fig. 1. **a** Cone-beam computed tomography during arterial portography (CBCTAP) shows hypoattenuating nodules in segments III (*arrow*) and IV (*arrowhead*). **b** On CBCT during hepatic arteriography (CBCTHA), both lesions show enhancement. Artifacts from the contrast material in the vessels are also seen. **c** Common hepatic arteriography shows a tumor stain in the left lobe of the liver (*arrow*). The tumor in segment IV is not demonstrated. **d** First, one branch of the anterior inferior subsegmental artery of the right hepatic artery was selected. Selective arteriography shows a tumor stain (*arrow*). Therefore, transcatheter arterial chemoembolization (TACE) was performed. **e** Subsequently, the tumor-feeding branch of the large tumor was selected, and TACE was performed. **f** Unenhanced CT performed 1 week after TACE shows dense iodized oil accumulation in both tumors

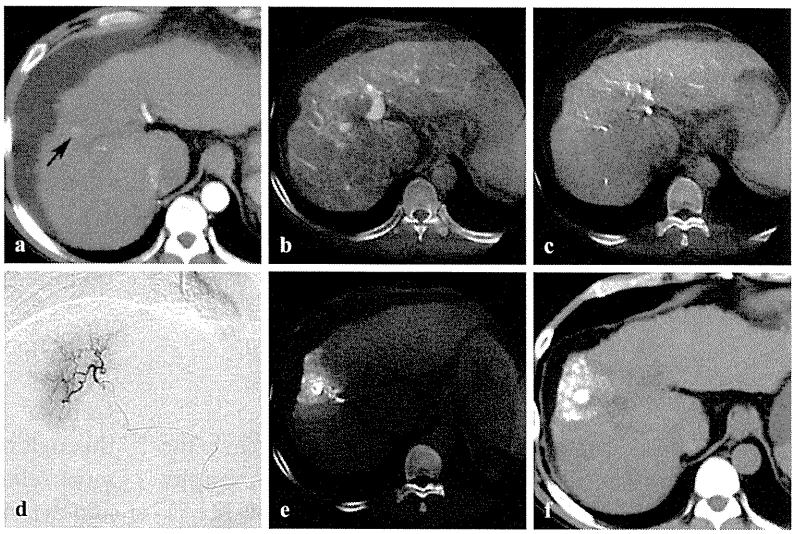

Fig. 2. **a** Arterial phase CT shows a small tumor in segment V (*arrow*). **b** On CBCTAP, the tumor is unclear. **c** It is also unclear on CBCTHA. **d** Based on the anatomical tumor location, a branch of the anterior inferior subsegmental artery of the right hepatic artery, suspected of being a tumor-feeding branch, was selected; and a mixture of iodized oil and anticancer drug was injected. **e** On CBCT after iodized oil injection (LipCBCT), the iodized oil was densely accumulated in the tumor with an adequate safety margin around the tumor. TACE was then completed. **f** Unenhanced CT performed 1 week after TACE shows dense iodized oil accumulation in the tumor

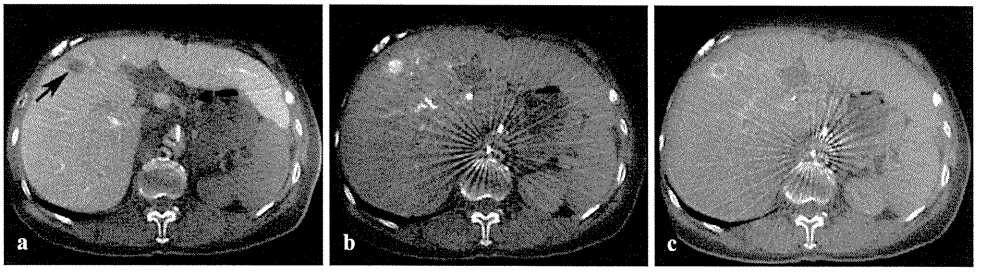

Fig. 3. **a** CBCTAP shows a small hypoattenuating nodule in segment V (*arrow*). **b** CBCTHA via the replaced right hepatic artery shows nodular enhancement. The radial artifacts from the catheter are also seen. **c** On second-phase CBCTHA, corona enhancement is clearly seen around the tumor

Fig. 4. **a** Coronal view of CBCTAP image shows a round, hypoattenuating area (*arrow*) and an amorphous hypoattenuating area in segment III (*arrowhead*). **b** On CBCTHA, both lesions show enhancement. **c** On second-phase CBCTHA, the round lesion shows corona enhancement, so the lesion is diagnosed as hepatocellular carcinoma (HCC). In contrast, the amorphous lesion shows prolonged enhancement without corona enhancement, and the lesion was diagnosed as an arterioportal shunt

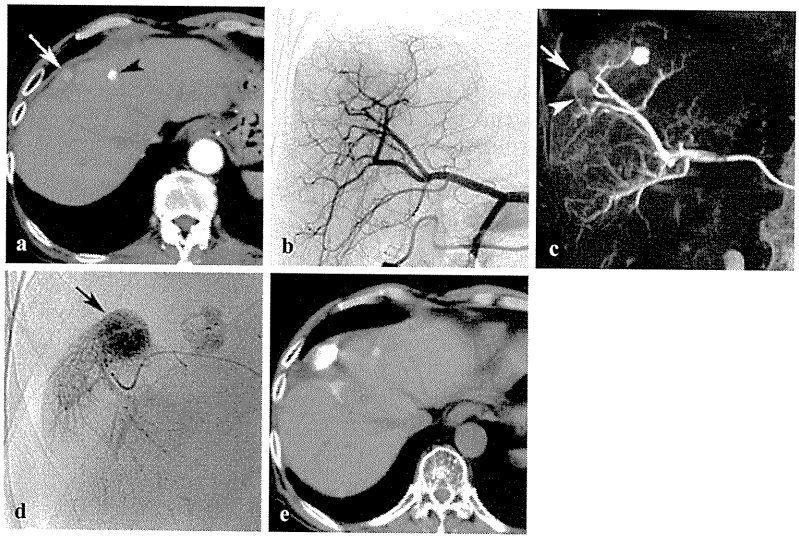

Fig. 5. **a** Arterial phase CT shows a small tumor in segment V (*arrow*). Another tumor that had previously been treated by TACE is also seen (*arrowhead*). **b** Common hepatic arteriography does not show any obvious tumor staining. **c** Oblique coronal maximum intensity projection (MIP) image from CBCTHA shows a tumor stain (*arrow*) fed by a small branch of the anterior inferior subsegmental artery of the right hepatic artery (*arrowhead*). **d** The branch was selected, and TACE was performed. The *arrow* indicates the tumor. **e** Unenhanced CT performed 1 week after TACE shows dense iodized oil accumulation in a limited area including the tumor

Fig. 6. **a** Arteriogram of the right hepatic artery shows a large tumor and an intrahepatic metastasis (*arrow*). Two branches were suspected of feeding the tumor (*arrowheads*). **b** First, a small branch of the posterior inferior subsegmental artery of the right hepatic artery was selected. Arteriography of this vessel shows a small tumor-feeding branch (*arrow*). **c** Sagittal view of CBCTHA image at this branch shows a partial tumor stain (*arrow*). Therefore, TACE was performed through this branch. **d** Second, the main feeding branch of the anterior inferior subsegmental artery of the right hepatic artery was selected, and TACE was performed. **e** Unenhanced CT performed 1 week after TACE shows dense iodized oil accumulation in the tumor and surrounding liver parenchyma

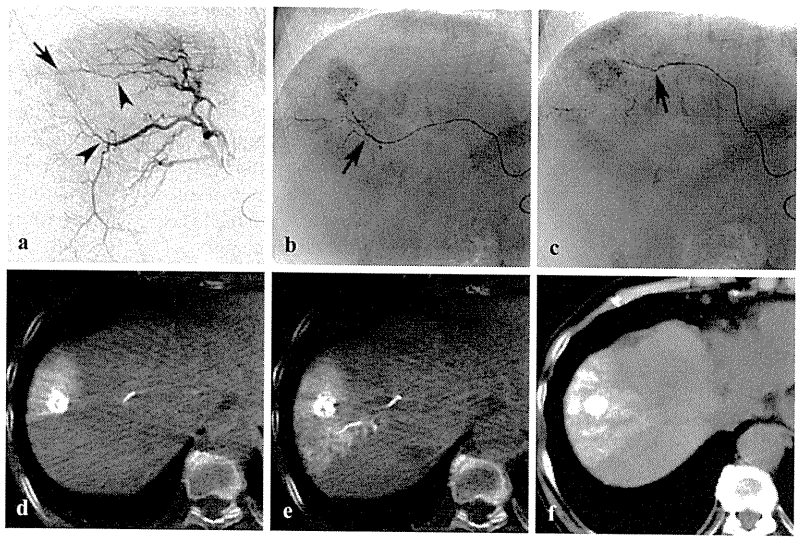

Fig. 7. **a** Arteriography of the anterior segmental artery of the right hepatic artery shows a faint tumor stain (*arrow*). Two branches were suspected of feeding the tumor (*arrowheads*). **b** First, one branch of the anterior inferior subsegmental artery was selected, and TACE was performed. The *arrow* shows the catheter tip. **c** Thereafter, the microcatheter was advanced into one branch of the anterior superior subsegmental artery and two-sequence CBCT was performed. The *arrow* shows the catheter tip. **d** The first scan obtained without contrast material injection shows that iodized oil does not distribute into the dorsal portion near the tumor. **e** The second scan obtained during injection of diluted contrast material through the microcatheter shows that contrast material distributes into the dorsal portion near the tumor. TACE was also performed at that point. **f** CT performed 1 week after TACE shows that the entire tumor is embolized with an adequate safety margin

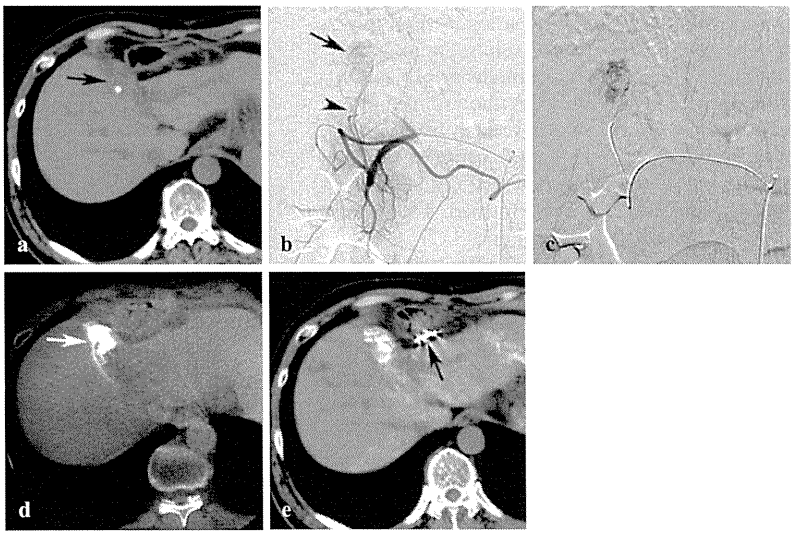

Fig. 8. **a** Unenhanced CT shows a recurrent tumor near the iodized oil accumulation in the previously treated tumor (*arrow*). **b** Arteriography of the gastroduodenal artery shows a tumor stain (*arrow*) supplied by the duodenal branch (*arrowhead*). **c** The tumor-feeding branch was selected. **d** CBCT at the embolization point shows a tumor stain (*arrow*). **e** Unenhanced CT performed 1 week after TACE shows iodized oil accumulation in the tumor. The *arrow* shows metallic coils placed in the right gastric artery to embolize another tumor (not shown)

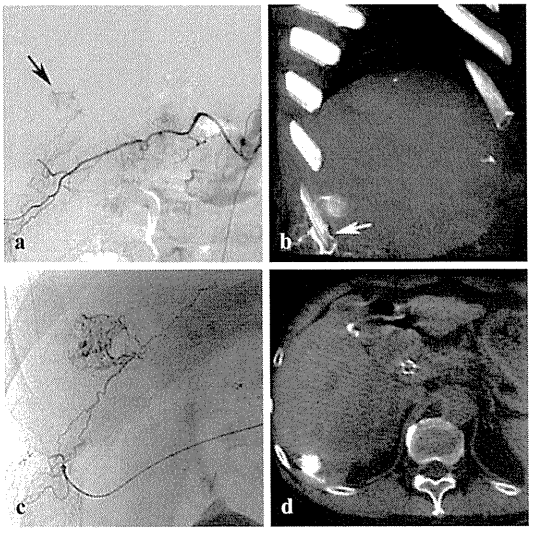

Fig. 9. **a** Arteriography of the right subcostal artery shows a tumor stain (*arrow*). **b** Sagittal view of an MIP image from CBCTA of the right subcostal artery shows a tumor-feeding branch with a sharp upward turn (*arrow*). **c** The microcatheter was advanced into the tumor-feeding branch, and TACE was performed. **d** CBCTHA at the embolization point does not show any enhancement of muscle tissues. Subsequently, TACE was performed

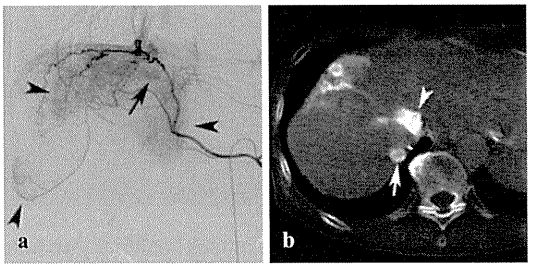

Fig. 10. **a** Arteriography of the right inferior phrenic artery shows a nodular stain (*arrow*) and amorphous stains (*arrowheads*). **b** CBCT during arteriography (CBCTA) at the right inferior phrenic artery shows a tumor in segment VII (*arrow*) and segmental enhancement of the caudate lobe (*arrowhead*)

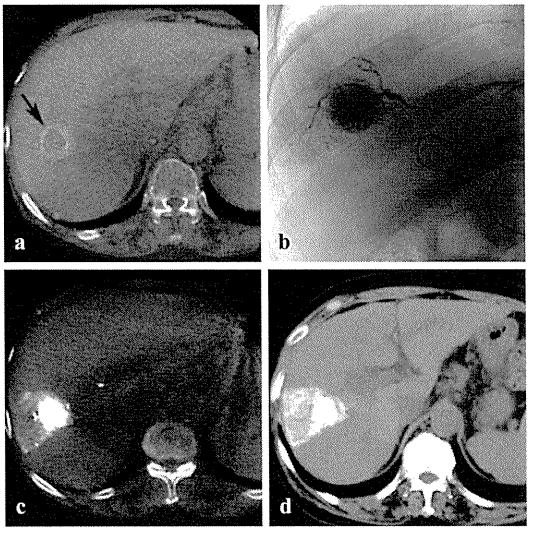

Fig. 11. **a** Second-phase CBCTHA shows a tumor with thick corona enhancement in segment V (*arrow*). **b** One branch of the anterior inferior subsegmental artery of the right hepatic artery was embolized. **c** LipCBCT shows dense iodized oil accumulation in the tumor with a safety margin. **d** Unenhanced CT performed 1 week after TACE also shows that the tumor is completely embolized

workstation can easily recognize the branching pattern of the feeder, and helpful information is provided for performing superselective catheterization (Fig. 5).

Confirmation of embolized area

Selective CBCTHA or LipCBCT at the embolization point can indicate the embolized area (Fig. 2).[10] Observation at the optimal direction of CBCT images is useful to confirm that the target tumor is entirely embedded in the embolized area with an adequate safety margin.

The HCC nodules frequently have multiple feeding branches. For large tumors, the main feeding branch should be embolized last because dense retention of iodized oil and contrast material in the tumor and liver parenchyma just after TACE makes it difficult to confirm the residual tumor.[1] CBCT can provide useful information for determining the order of embolization for each feeder (Fig. 6). In contrast, for small tumors, the order of embolization of each feeder is not strict because artifacts from iodized oil and contrast material do not reduce the image quality as much (Fig. 7).

The two-sequence CBCT technique without and with contrast material injection is also useful for confirming each embolized area of two vessels during TACE when the tumor is supplied by two feeding branches (Fig. 7). After embolization of one feeding branch, the catheter is advanced into the other feeding branch. The first scan is then obtained without contrast material injection, followed by the second scan after contrast material is injected through the catheter. The first CBCT images depict the iodized oil distribution in the vascular territory of the feeding branch that was embolized immediately before the scan, and the second set of CBCT images indicate the vascular territory of the other feeding branch just selected by the catheter. This technique may improve the technical success rates of ultraselective TACE and may reduce the effort and procedural duration. If the scan becomes faster, it will become possible to obtain these two sequential images during a single breath-hold.

Prevention of nontarget embolization

TACE through extrahepatic vessels may cause severe complications when a nontarget branch is embolized.[2–5] CBCTA through extrahepatic collateral vessels is useful for avoiding nontarget embolization (Figs. 8, 9). When CBCTA shows enhancement of the nontumor tissues as well as tumor staining, the catheter should be distally advanced into the tumor-feeding branch to prevent unnecessary embolization of vessels that do not supply the tumor (Fig. 9). In addition, CBCTA is useful for distinguishing between tumor staining and nontumor staining, which is seen most frequently with arteriography of the inferior phrenic artery (Fig. 10).

Recognition of endpoints of TACE

The goal of TACE for HCC is that the target tumor is embolized with an adequate safety margin (Fig. 11). CBCT can confirm that the endpoint of TACE has been reached. Local control effects of TACE may be improved and adverse effects reduced when intraprocedural monitoring of embolized areas is performed by CBCT.

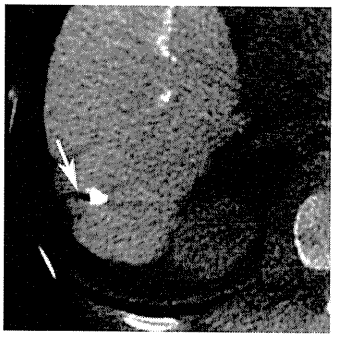

Fig. 12. On CBCTAP, note the artifacts from densely concentrated iodized oil (*arrow*)

In a previous report, 82% of small HCCs that could not be detected by angiography could be embolized with an adequate safety margin at least 5 mm wide using two to six (mean 3.8 ± 1.1) CBCT procedures.[10]

Limitations of CBCT

An advantage of CBCT technology is that it can reduce the irradiation dose compared to that used during conventional CT.[7] There are also some disadvantages. CBCT images have several noises, in particular at the central portion of the FOV. In addition, CBCT images are low contrast, and motion artifacts mainly caused by inadequate breath-holding deteriorates the image quality. Artifacts from the catheter, contrast material in the vessels, or densely accumulated iodized oil are also seen (Figs. 1, 3, 12).[9] An advanced algorithm and a faster scanning protocol to reduce these image artifacts may be needed to improve the image quality. The FOV of CBCT is also too small to observe the entire liver.[9] HCC nodules located in the lateral segment of the liver are not included in the FOV of CBCT in large patients when the right lobe of the liver is entirely included in the FOV.

Conclusion

Cone-beam computed tomography using an FPD is an alternative method of obtaining cross-sectional images. The image quality of CBCT is low compared to that of conventional CT, but CBCT provides useful information about performing TACE for HCC safely and effectively with little effort.

References

1. Miyayama S, Matsui O, Yamashiro M, Ryu Y, Kaito K, Ozaki K, et al. Ultraselective transcatheter arterial chemoembolization with a 2-F tip microcatheter for small hepatocellular carcinomas: relationship between local tumor recurrence

and visualization of the portal vein with iodized oil. J Vasc Interv Radiol 2007;18:365–76.
2. Takayasu K, Moriyama N, Muramatsu Y, Shima Y, Ushio K, Yamada T, et al. Gallbladder infarction after hepatic artery embolization. AJR Am J Roentgenol 1985;144:135–8.
3. Arora R, Soulen MC, Haskal ZJ. Cutaneous complications of hepatic chemoembolization via extrahepatic collaterals. J Vasc Interv Radiol 1999;10:1351–6.
4. Kim HC, Chung JW, Lee W, Jae HJ, Park JH. Recognizing extrahepatic collateral vessels that supply hepatocellular carcinoma to avoid complications of transcatheter arterial chemoembolization. Radiographics 2005;25:S25–39.
5. Miyayama S, Matsui O, Taki K, Minami T, Ryu Y, Ito C, et al. Extrahepatic blood supply to hepatocellular carcinoma: angiographic demonstration and transcatheter arterial chemoembolization. Cardiovasc Intervent Radiol 2006;29:39–48.
6. Takayasu K, Muramatsu Y, Maeda T, Iwata R, Furukawa H, Muramatsu Y, et al. Targeted transarterial oily chemoembolization for small foci of hepatocellular carcinoma using a unified helical CT and angiography system: analysis of factors affecting local recurrence and survival rates. AJR Am J Roentogenol 2001;176:681–8.
7. Hirota S, Nakao N, Yamamoto S, Kobayashi K, Maeda H, Ishikawa R, et al. Cone-beam CT with flat-panel-detector digital angiography system: early experience in abdominal interventional procedures. Cardiovasc Intervent Radiol 2006;29:1034–8.
8. Kakeda S, Korogi Y, Ohnari N, Moriya J, Oda N, Nishino K, et al. Usefulness of cone-beam CT with flat panel detectors in conjunction with catheter angiography for transcatheter arterial embolization. J Vasc Interv Radiol 2007;18:1508–16.
9. Miyayama S, Matsui O, Yamashiro M, Ryu Y, Takata H, Takeda T, et al. Detection of hepatocellular carcinoma by CT during arterial portography using a cone-beam CT technology: comparison with conventional CTAP. Abdom Imaging 2009;34:502–6.
10. Miyayama S, Yamashiro M, Okuda M, Yoshie Y, Sugimori N, Igarashi S, et al. Usefulness of cone-beam computed tomography during ultraselective transcatheter arterial chemoembolization for small hepatocellular carcinomas that cannot be demonstrated on angiography. Cardiovasc Intervent Radiol 2009;32:255–64.
11. Tognolini A, Louie JD, Hwang GL, Hofmann LV, Sze DY, Kothary N. Utility of C-arm CT in patients with hepatocellular carcinoma undergoing transhepatic arterial chemoembolization. J Vasc Interv Radiol 2010;21:339–47.
12. Miyayama S, Yamashiro M, Okuda M, Yoshie Y, Nakashima Y, Ikeno H, et al. Detection of corona enhancement of hypervascular hepatocellular carcinoma by C-arm dual-phase cone-beam CT during hepatic arteriography. Cardiovasc Intervent Radiol 2011;34:81–6.
13. Ueda K, Matsui O, Kawamori Y, Nakanuma Y, Kadoya M, Yoshikawa J, et al. Hypervascular hepatocellular carcinoma: evaluation of hemodynamics with dynamic CT during hepatic arteriography. Radiology 1998;206:161–6.
14. Kitao A, Zen Y, Matsui O, Gabata T, Nakanuma Y. Hepatocarcinogenesis: multistep changes of drainage vessels at CT during arterial portography and hepatic arteriography—radiologic-pathologic correlation. Radiology 2009;252:605–14.
15. Ueda K, Matsui O, Kawamori Y, Kadoya M, Yoshikawa J, Gabata T, et al. Differentiation of hypervascular hepatic pseudolesions from hepatocellular carcinoma: value of single-level dynamic CT during hepatic arteriography. J Comput Assist Tomogr 1998;22:703–8.

Cardiovasc Intervent Radiol
DOI 10.1007/s00270-011-0328-2

CLINICAL INVESTIGATION

Origins of Feeding Arteries of Hepatocellular Carcinoma Located Near the Umbilical Fissure of the Left Hepatic Lobe: Angiographic Evaluation

Shiro Miyayama · Masashi Yamashiro · Yoshihiro Shibata · Masahiro Hashimoto · Miki Yoshida · Kazunobu Tsuji · Fumihito Toshima · Osamu Matsui

Received: 3 October 2011 / Accepted: 23 November 2011

Abstract
Purpose To analyze the origins of the feeding arteries of hepatocellular carcinomas (HCCs) near the umbilical fissure of the left hepatic lobe.
Methods Twenty-eight HCCs with a mean ± SD tumor diameter of 3.4 ± 1.0 cm (range 1–4.4 cm) in contact with the right or left side of the umbilical fissure were treated by superselective transcatheter arterial chemoembolization (TACE). The origins of the tumor-feeding arteries were analyzed with arteriograms and computed tomography or cone-beam computed tomography images obtained during and 1 week after TACE.
Results Twenty-one HCC lesions were located in segment 3 and seven were located in segment 4. Of 21 tumors in segment 3, 13 (61.9%) were supplied by the lateral inferior subsegmental artery (A3), three (14.3%) by the medial subsegmental artery (A4), three (14.3%) by both A4 and A3, one (4.8%) by a branch arising from the left lateral hepatic artery, and one (4.8%) by a branch of the right gastric artery. In particular, all tumor-feeding branches arising from A4 were the first branch of A4. Of seven tumors in segment 4, four (57.1%) were supplied by A4 and three (42.9%) by A3. In particular, all tumor-feeding branches arising from A3 were the first branch of A3.
Conclusion This study demonstrates crossover blood supply to HCC lesions located near the umbilical fissure, in addition to direct feeding from a separate branch. In particular, the first branch of the opposite subsegmental artery may feed tumors when crossover blood supply is present.

Keywords Feeding artery · Hepatocellular carcinoma · Transcatheter arterial chemoembolization · Umbilical fissure

Introduction

Transcatheter arterial chemoembolization (TACE) is one of the most effective treatments for inoperable hepatocellular carcinoma (HCC), and it is performed worldwide [1–4]. Superselective catheterization into the tumor-feeding branches with a microcatheter is essential to enhance the therapeutic effects and to reduce the adverse effects of TACE [2–4].

The left hepatic lobe is divided into the medial and lateral segments by the umbilical fissure, which consists of the parietal surface of the falciform ligament attachment and the visceral surface of the fissure for the ligamentum venosum and ligamentum teres [5–7]. However, it is reported that small branches of the bile duct and vessels infrequently cross the umbilical fissure [7–10]. Therefore, it is important to recognize the arterial blood supply to HCC lesions near the umbilical fissure to perform effective TACE.

The purpose of this study was to evaluate the origins of the feeding arteries of HCCs located near the umbilical fissure.

Materials and Methods

We retrospectively analyzed the origins of the feeding arteries of HCCs near the umbilical fissure. Institutional

S. Miyayama (✉) · M. Yamashiro · Y. Shibata · M. Hashimoto · M. Yoshida · K. Tsuji · F. Toshima
Department of Diagnostic Radiology, Fukuiken Saiseikai Hospital, 7-1, Funabashi, Wadanaka-cho, Fukui 918-8503, Japan
e-mail: s-miyayama@fukui.saiseikai.or.jp

O. Matsui
Department of Radiology, Kanazawa University Graduate School of Medical Science, 13-1, Takara-machi, Kanazawa 920-8641, Japan

Published online: 16 December 2011

review board approval is not required at our institution for this type of study. Written informed consent was obtained from each patient before the TACE procedure.

Patients

We selected newly developed HCCs <5 cm in diameter in contact with the right or left surface of the umbilical fissure (Fig. 1), not extending over both sides of the umbilical fissure, and treated by superselective TACE. Although we are well aware that the umbilical fissure is present between segments 2 and 4, tumors located in segment 2 and in the cranial part of segment 4 were excluded from the present study because the falciform ligament was not always outlined clearly on computed tomography (CT) at the cranial part of the left hepatic lobe. We also excluded HCCs that were locally recurrent tumors after previous treatment including TACE, HCCs that were newly developed but for which TACE to segments 3 and 4 had previously been performed, and HCCs that were initially treated by TACE at the left hepatic artery level in a nonselective fashion. Between October 2001 and July 2011, a total of 28 HCC lesions in 28 patients met the above criteria. There were 18 men and 10 women in the study with a mean ± SD patient age of 71.3 ± 9.1 years (range 56–89 years). All patients had chronic hepatitis or liver cirrhosis. This was related to hepatitis C in 22 patients and hepatitis B in two patients. The etiology was unknown in four patients. Fifteen patients had no history of any treatment for HCC. Thirteen patients had previously undergone 1–8 TACE sessions (3.2 ± 2.1) for HCCs except for segments 3 and 4.

All patients had a single HCC lesion located near the umbilical fissure with a mean tumor diameter of 3.4 ± 1.0 cm (range 1–4.4 cm). Fourteen patients also had other viable HCC lesions besides the tumor near the umbilical fissure. The diagnosis of HCC was made by imaging findings: nodular staining and washout on dynamic CT and/or dynamic magnetic resonance imaging; nodular staining on arteriography and/or CT during hepatic arteriography; and nodular perfusion defect on CT during arterial portography, in addition to hyperintensity on T2-weighted and diffusion-weighted magnetic resonance imaging.

TACE Procedure

TACE was performed at the more distal level to the subsegmental artery through a 1.8–2.4F tip microcatheter (Carnelian Pixie ER; Tokai Medical Products, Kasugai, Japan, Progreat α, Σ; Terumo, Tokyo, Japan; and Microferret-18; Cook, Bloomington, IN) with 2–4 ml of iodized oil (Lipiodol; Andre Guerbet, Aulnaysous-Bois, France) and anticancer drugs (10–20 mg of epirubicin [Farmorbicin; Pfizer, Tokyo, Japan] and 2–4 mg of mitomycin C [Mitomycin; Kyowa Hakko Kirin, Tokyo, Japan]), followed by approximately 0.2–0.5-mm gelatin sponge particles (Gelfoam; Upjohn, Kalamazoo, MI; or Gelpart; Nippon Kayaku, Tokyo, Japan). Selective CT or cone-beam CT (CBCT) examination at the TACE point was also performed if necessary. Unenhanced CT was routinely obtained 1 week after TACE to check for the distribution of the iodized oil injected during TACE.

Assessment

The findings of arteriograms, CT, or CBCT obtained during TACE and CT obtained 1 week after TACE were analyzed to confirm the origins of the feeding arteries of HCCs located near the umbilical fissure. The embolized artery was confirmed as the tumor-feeding artery when selective arteriogram, CT, and/or CBCT demonstrated tumor staining and iodized oil accumulation in the tumor was observed on CT obtained 1 week after TACE.

Results

Twenty-one HCC lesions (75%) were located at the left side of the umbilical fissure (segment 3) (Figs. 2, 3, 4, 5),

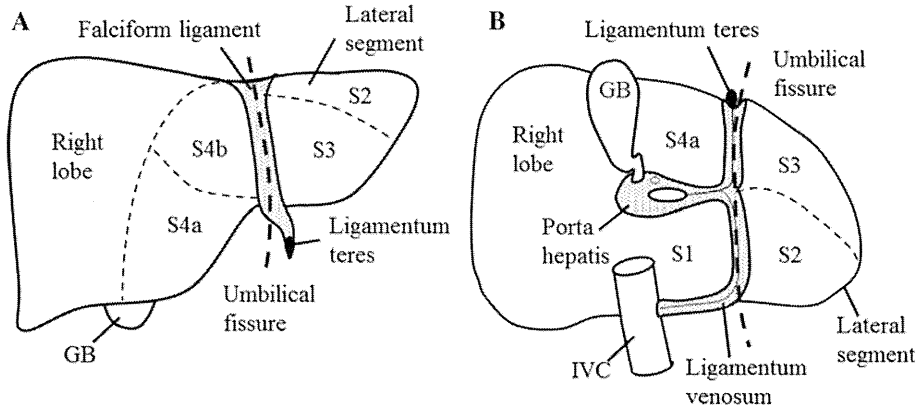

Fig. 1 Schematic presentation of the umbilical fissure. **A** Frontal view. **B** Caudal view. *GB* gallbladder, *S1* segment 1, *S4* segment 4, *IVC* inferior vena cava. The umbilical fissure is identified as a fat plane between S4 and the lateral segment on CT

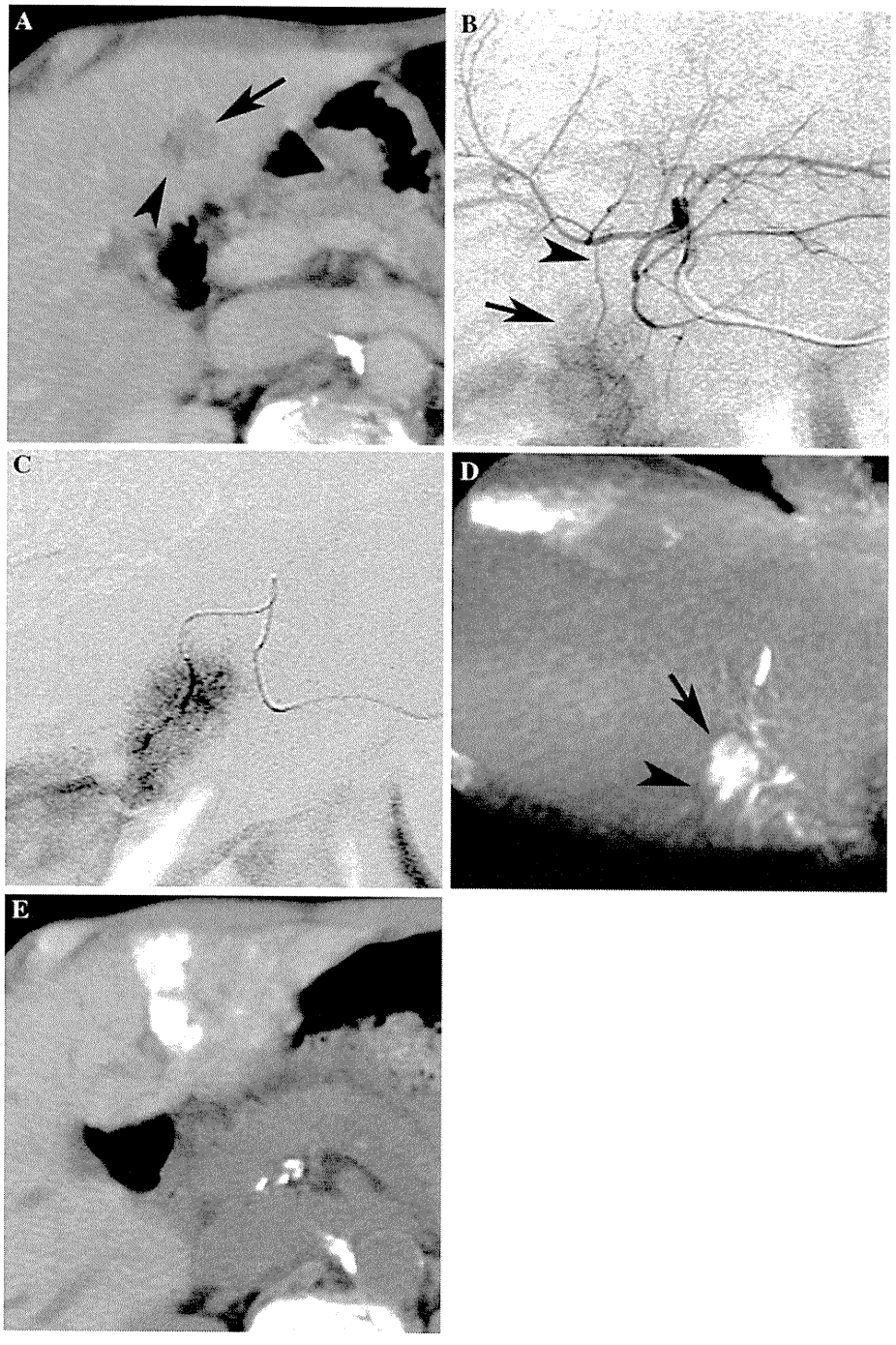

Fig. 2 HCC located at the left side of the umbilical fissure in an 80-year-old man. **A** CT revealed a tumor (*arrow*) at the left side of the umbilical fissure (*arrowhead*). **B** Left hepatic arteriogram revealed tumor staining (*arrow*) supplied by the first branch derived from the medial subsegmental artery (A4) (*arrowhead*). **C** Selective arteriogram of the branch revealed tumor staining. TACE was performed at this point. **D** Oblique coronal view of CBCT obtained immediately after TACE of the branch revealed iodized oil accumulation in a tumor (*arrow*) located at the left side of the umbilical fissure (*arrowhead*). Another tumor that was simultaneously embolized was observed in the right hepatic lobe. **E** CT obtained 1 week after TACE revealed dense iodized oil accumulation in a limited area at the left side of the umbilical fissure including the tumor

and seven (25%) were located at the right side of the umbilical fissure (segment 4) (Fig. 6).

Of 21 HCC lesions in segment 3, 13 tumors (61.9%) were supplied by the lateral inferior subsegmental artery (A3), three (14.3%) were supplied by the medial subsegmental artery (A4) (Fig. 2), three (14.3%) were supplied by both A4 and A3 (Fig. 3), one (4.8%) was supplied by a branch directly arising from the left lateral hepatic artery (Fig. 4), and one (4.8%) was supplied by a branch arising from the right gastric artery (Fig. 5). In particular, all tumor-feeding branches arising from A4 were the first branch of A4 (Figs. 2, 3).

Of seven HCC lesions in segment 4, four tumors (57.1%) were supplied by A4 and three (42.9%) were supplied by A3 (Fig. 6). In particular, all tumor-feeding branches arising from A3 were the first branch of A3 (Fig. 6).

There were no anastomoses between any tumor-feeding branches arising from the opposite subsegmental artery and the arterial branches of the tumor-bearing subsegment.

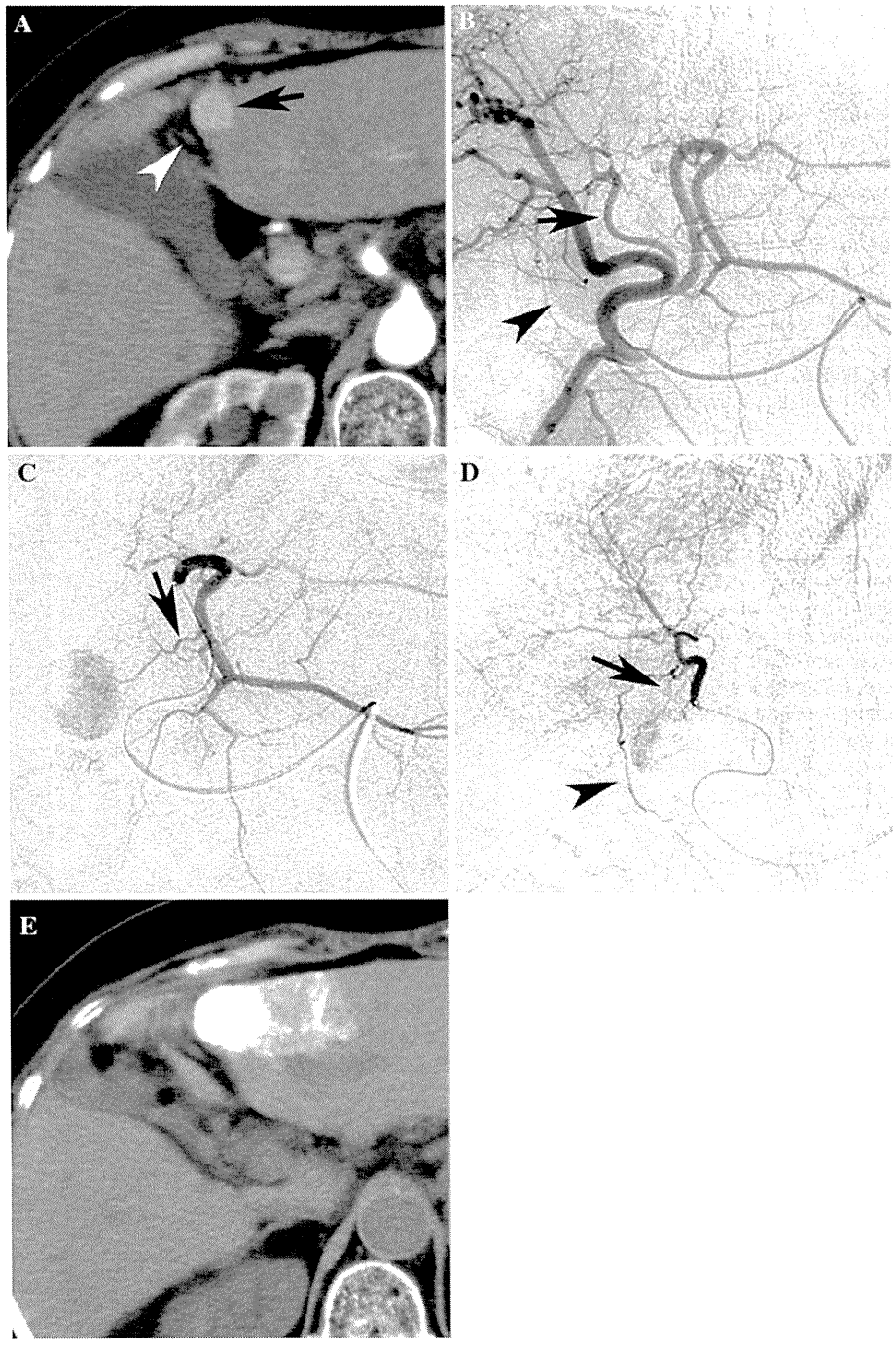

Fig. 3 HCC located at the left side of the umbilical fissure in a 70-year-old woman. **A** CT revealed a tumor (*arrow*) at the left side of the umbilical fissure (*arrowhead*). **B** Common hepatic arteriogram revealed that A4 arose as the middle hepatic artery (*arrow*). The *arrowhead* indicates tumor staining. **C** Lateral left hepatic arteriogram revealed that the tumor was mainly supplied by the first branch of the lateral inferior subsegmental artery (A3) (*arrow*). **D** Middle hepatic arteriogram also revealed staining at the right side of the tumor supplied by the first branch of A4. The falciform artery was also seen (*arrowhead*). **E** CT obtained 1 week after TACE revealed dense iodized oil accumulation in the tumor

Discussion

Liver segments, as defined by Couinaud [5], are generally used to describe segmental anatomy. The umbilical fissure, which is the left intersegmental plane, anatomically divides the left hepatic lobe into the medial and lateral segments [5–8]. Therefore, the right side of the umbilical fissure is included in segment 4 and the left side is included in segments 2 and 3.

In a cadaver study by Gupta et al. [7], small branches of the medial segmental duct and blood vessels crossed to the left of the umbilical fissure in 4.7% cases and the lateral segmental duct and blood vessels crossed to the right of the umbilical fissure in 2.4%. Renz et al. [9] reported that biliary radicles originating from segment 4 were identified as crossing the umbilical fissure in 30% of cases. In the present study, the branch of A4 partially or completely supplied 28.6% of HCC lesions in segment 3 near the

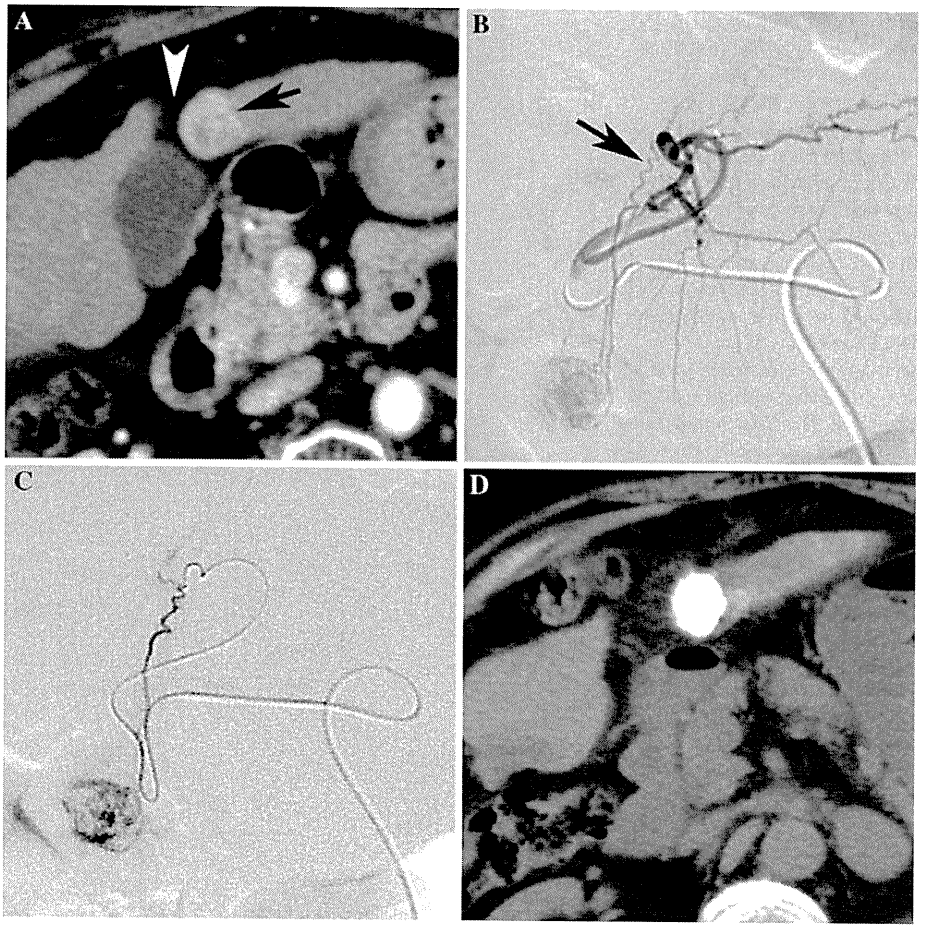

Fig. 4 HCC located at the left side of the umbilical fissure in a 71-year-old woman. **A** CT revealed a tumor (*arrow*) at the left side of the umbilical fissure (*arrowhead*). **B** Lateral left hepatic arteriogram revealed that the tumor was supplied by a branch directly arising from the lateral segmental artery before the bifurcation of A2 and A3 (*arrow*). **C** Selective arteriogram of the branch revealed tumor staining. **D** CT obtained 1 week after TACE revealed dense iodized oil accumulation in the tumor

umbilical fissure, while the branch of A3 completely supplied 42.9% of HCC lesions in segment 4 near the umbilical fissure. The incidences of crossover blood supply in our results were higher than those of the cadaver or surgical studies. This suggests that small tumor-feeding branches crossing the umbilical fissure become apparent in HCC lesions because the tumors are hypervascular and the feeding branches are usually hypertrophied. In a study by Chen et al. [11] that used carbon dioxide (CO_2)-enhanced ultrasonography during hepatic arteriography, crossover blood supply between the medial and left lateral segments was seen in 50% (7 of 14) of cases. However, CO_2 may pass through tiny arterioportal communications that cannot be demonstrated on arteriograms using iodinated contrast medium because of its extremely low viscosity [12]. Therefore, it may be impossible to determine whether CO_2 is distributed into the opposite liver parenchyma via the artery or portal vein. In addition, intersegmental arterial communications between the medial and left lateral segments are extrahepatically located in the umbilical plate [10]. If the catheter is not deeply advanced into the segmental artery, CO_2 may also pass through these intersegmental arterial communications and flow into the opposite liver parenchyma.

In the present study, all tumor-feeding branches arising from the opposite subsegmental artery were the first branch of each subsegmental artery without anastomosis. Cho et al. [10] also reported that the left lateral hepatic artery forked off into branches that crossed the umbilical portion and nourished the liver parenchyma of segment 4 without communicating with the middle hepatic artery in 25% (3 of 12) of cases. Our study suggests that crossover arterial supply between segments 3 and 4 without anastomosis is not clinically rare, not only from segment 3 to segment 4, but also from segment 4 to segment 3.

Additionally, two HCC lesions in segment 3 near the umbilical fissure were supplied by a separate feeding branch arising from the left lateral hepatic artery or right gastric artery. To our knowledge, there are no reports demonstrating this peculiar vascular anatomy supplying a small part of segment 3 near the umbilical fissure.

There is a significant limitation to the present study. We only evaluated crossover blood supply between segments 3 and 4 in patients with HCC near the umbilical fissure. The

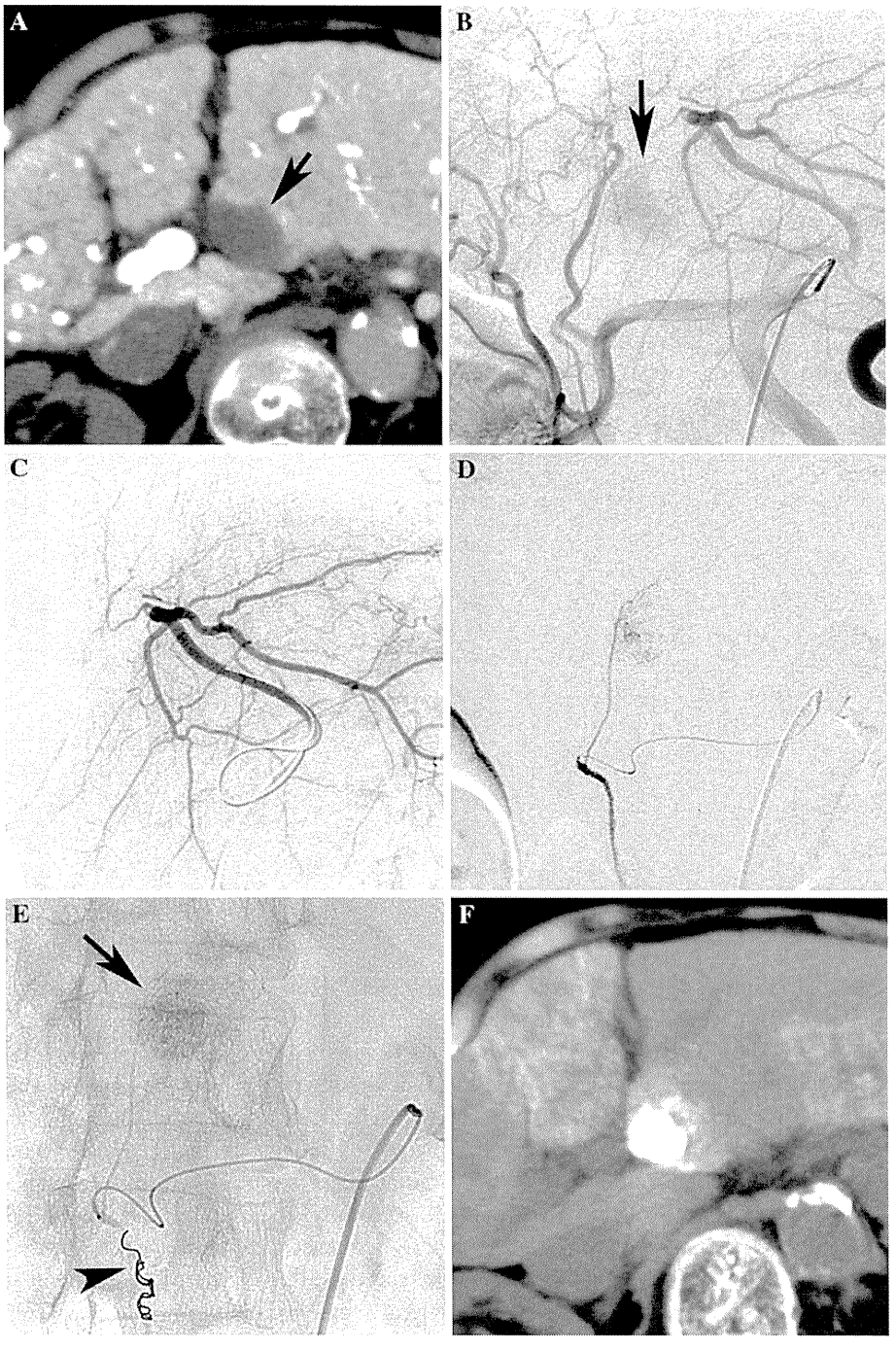

Fig. 5 HCC located at the left side of the umbilical fissure in an 86-year-old woman. **A** CT during arterial portography revealed a tumor at the left side of the umbilical fissure (*arrow*). **B** Celiac arteriogram revealed tumor staining (*arrow*). The left lateral hepatic artery arose from the left gastric artery. **C** Left lateral hepatic arteriogram revealed no tumor staining. **D** Oblique view of an arteriogram of the right gastric artery revealed a small feeding branch. **E** The branch could not be selected, so TACE was performed after embolization of the right gastric artery with microcoils (*arrowhead*). The *arrow* indicates an iodized oil-accumulated tumor. **F** CT obtained 1 week after TACE revealed dense iodized oil accumulation in the tumor. Iodized oil was also distributed into segments 2 and 4 because additional TACE was subsequently performed on other tumors (not shown)

incidences of crossover blood supply in the present study may not reflect the natural anatomic conditions because HCC lesions usually tend to parasitize the neighboring arteries as a result of their hypervascularity. Therefore, tumor location and size might strongly influence the incidence of crossover blood supply to HCC lesions. However, we believe that our results are clinically important to appropriately select the feeding branch of tumors located near the umbilical fissure, especially when a tumor is small and its staining is faint on arteriography.

In conclusion, the present study demonstrated crossover blood supply to HCC lesions located near the umbilical fissure in addition to direct feeding from the left lateral hepatic artery or right gastric artery. When the crossover blood supply was present, the first branch of the opposite subsegmental artery fed the tumor. We think that our

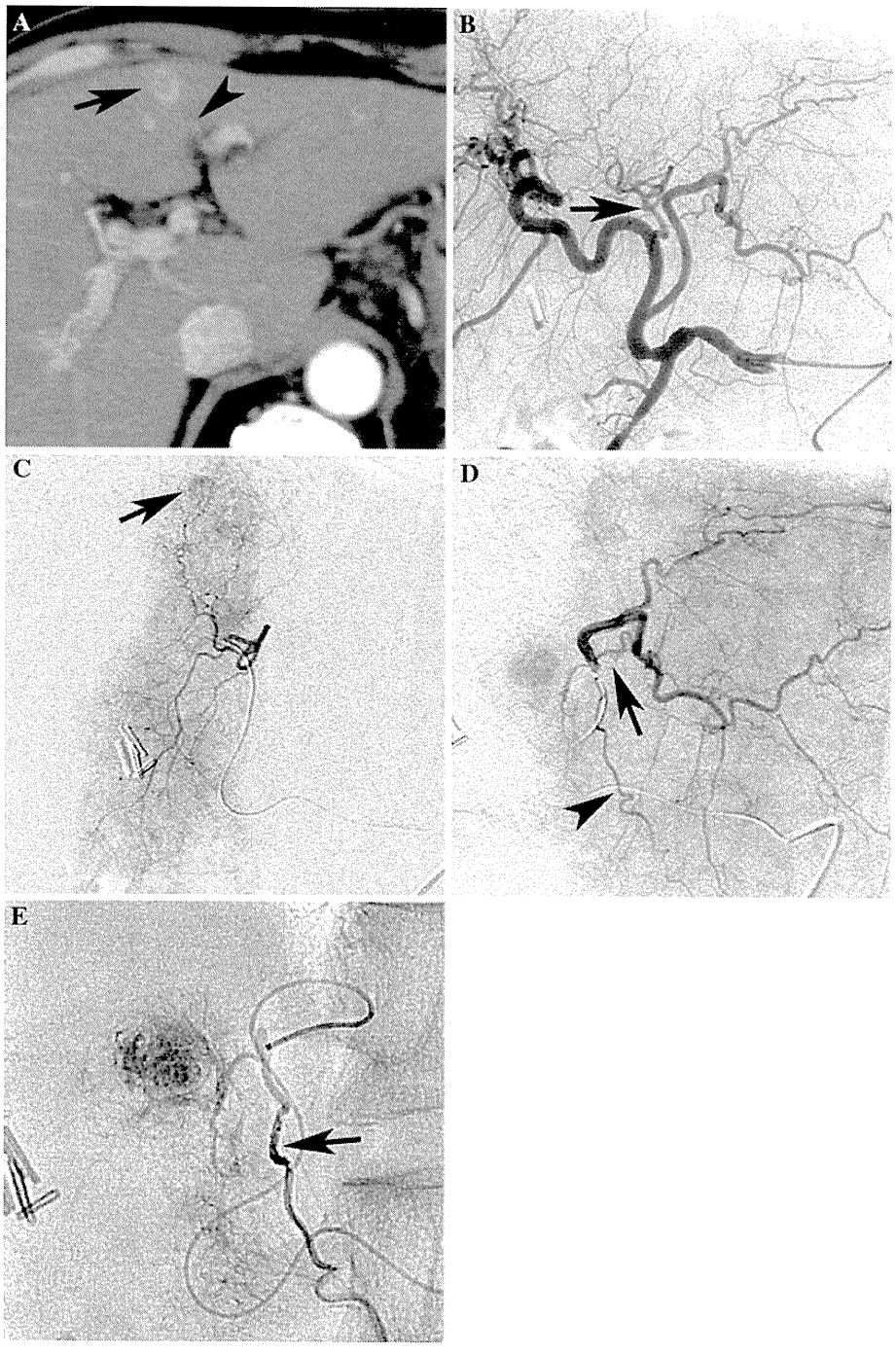

Fig. 6 HCC located at the right side of the umbilical fissure in a 58-year-old man. **A** CT revealed a tumor (*arrow*) at the right side of the umbilical fissure (*arrowhead*). **B** Common hepatic arteriogram revealed that A4 arose as the middle hepatic artery (*arrow*). **C** Middle hepatic arteriogram revealed no obvious staining corresponded to the tumor near the umbilical fissure. A small tumor was demonstrated at another site (*arrow*). **D** Lateral left hepatic arteriogram revealed tumor staining supplied by the first branch of A3. The falciform artery also arose from this branch (*arrowhead*). **E** TACE was performed after embolization of the falciform artery with microcoils (*arrow*)

results are important to perform effective TACE for HCC lesions located near the umbilical fissure.

Conflict of interest The authors declare that they have no conflict of interest.

References

1. Yamada R, Sato M, Kawabata M et al (1983) Hepatic artery embolization in 120 patients with unresectable hepatoma. Radiology 148:397–401
2. Uchida H, Ohishi H, Matsuo N et al (1990) Transcatheter hepatic segmental arterial embolization using lipiodol mixed with an anticancer drug and Gelfoam particles for hepatocellular carcinoma. Cardiovasc Intervent Radiol 13:140–145
3. Matsui O, Kadoya M, Yoshikawa J et al (1993) Small hepatocellular carcinoma: treatment with subsegmental transcatheter arterial embolization. Radiology 188:79–83
4. Miyayama S, Matsui O, Yamashiro M et al (2007) Ultraselective transcatheter arterial chemoembolization with a 2-F tip microcatheter for small hepatocellular carcinomas: relationship between local tumor recurrence and visualization of the portal vein with iodized oil. J Vasc Interv Radiol 18:365–376

5. Couinaud C (1954) Lobes et segments hépatiques: notes sur l'architecture anatomique et chirurgicale du foie. Presse Med 62:709–712
6. Bismuth H (1982) Surgical anatomy and anatomical surgery of the liver. World J Surg 6:3–9
7. Gupta SC, Gupta CD, Arora AK (1977) Subsegmentation of the human liver. J Anat 124:413–423
8. Reichert PR, Renz JF, D'Albuquerque LAC et al (2000) Surgical anatomy of the left lateral segment as applied to living-donor and split-liver transplantation: a clinicopathologic study. Ann Surg 232:658–664
9. Renz JF, Reichert PR, Emond JC (2000) Biliary anatomy as applied to pediatric living donor as split-liver transplantation. Liver Transplant 6:801–804
10. Cho A, Gunji H, Koike N et al (2007) Intersegmental arterial communication between the medial and left lateral segments of the liver. Dig Surg 24:328–330
11. Chen RC, Chou CT, Chen WT et al (2011) Delineation of the watershed between right and left hepatic arterial territories with carbon dioxide-enhanced ultrasonography. J Vasc Interv Radiol 22:667–672
12. Takeda T, Ido K, Yuasa Y et al (1988) Intraarterial digital subtraction angiography with carbon dioxide: superior detectability of arteriovenous shunting. Cardiovasc Intervent Radiol 11:101–107

Jpn J Radiol
DOI 10.1007/s11604-011-0043-6

ORIGINAL ARTICLE

Comparison of local control effects of superselective transcatheter arterial chemoembolization using epirubicin plus mitomycin C and miriplatin for hepatocellular carcinoma

Shiro Miyayama · Masashi Yamashiro · Yoshihiro Shibata · Masahiro Hashimoto · Miki Yoshida · Kazunobu Tsuji · Fumihito Toshima · Osamu Matsui

Received: 7 September 2011 / Accepted: 5 December 2011

Abstract
Purpose To compare local control effects of superselective transcatheter arterial chemoembolization (TACE) using epirubicin (EPI) plus mitomycin C (M) and miriplatin (MPT) for hepatocellular carcinoma (HCC).
Materials and methods One-hundred and twenty-nine HCCs treated with superselective TACE were divided into three groups according to the type of anticancer drug; EPI-M-TACE ($n = 51$), MPT-TACE ($n = 21$), and MPT-I-TACE (MPT emulsion) ($n = 57$). Local recurrence, patterns of recurrence (intratumoral recurrence; IR), and follow-up angiograms were evaluated.
Results Mean tumor diameter and follow-up period for the EPI-M-TACE, MPT-TACE, and MPT-I-TACE groups were 16.9 mm and 15.5 months, 20.7 mm and 12.0 months, and 18.8 mm and 9.6 months, respectively. Local recurrence for the EPI-M-TACE, MPT-TACE, and MPT-I-TACE groups at 5, 10, and 15 months was 6.1, 47.6, and 40.1%, 23.5, 67.3, and 63.9%, and 26.2, 75.4, and 72.9%, respectively. IR for the EPI-M-TACE, MPT-TACE, and MPT-I-TACE groups was 23.1, 71.4, and 71.0%, respectively. Local recurrence and IR in the EPI-M-TACE group were significantly less than those in the MPT-TACE and MPT-I-TACE groups. Follow-up angiograms revealed less arterial damage in the MPT-TACE and MPT-I-TACE groups.
Conclusion Superselective TACE using MPT resulted in very frequent local recurrence, in particular IR, despite less arterial damage.

Keywords Hepatocellular carcinoma · Transcatheter arterial chemoembolization · Miriplatin · Local recurrence

Introduction

Transcatheter arterial chemoembolization (TACE) is an effective therapeutic option for inoperable hepatocellular carcinoma (HCC) [1–4]. With advances in microcatheter and guidewire technology, the tumor-feeding branch can be selected in almost all patients and local control effects of TACE have been improved [2–4]. It is generally believed that the antitumoral effects of superselective TACE depend mainly on the ischemic effects of the embolic materials, and the importance of anticancer drugs is uncertain.

The anticancer drug miriplatin (MPT; Miripla; Dainippon Sumitomo, Osaka, Japan) is a lipophilic platinum complex [5, 6]. It has been developed as a new drug for use in transcatheter arterial infusion (TAI) for HCC [7]. Recently, it has also been used in TACE [8], however, the therapeutic effects of MPT in TACE have not been established.

Thus, the purpose of this study was to retrospectively evaluate the local control effects of superselective TACE for HCC using MPT compared with that using epirubicin (EPI; Farmorubicin; Pfizer, Tokyo, Japan) plus mitomycin C (M; Mitomycin; Kyowa Hakko Kirin, Tokyo, Japan).

S. Miyayama (✉) · M. Yamashiro · Y. Shibata · M. Hashimoto · M. Yoshida · K. Tsuji · F. Toshima
Department of Diagnostic Radiology, Fukuiken Saiseikai Hospital, 7-1 Funabashi, Wadanaka-cho, Fukui 918-8503, Japan
e-mail: s-miyayama@fukui.saiseikai.or.jp

O. Matsui
Department of Radiology, Kanazawa University Graduate School of Medical Science, 13-1 Takara-machi, Kanazawa 920-8641, Japan

Published online: 07 January 2012

Materials and methods

Our institutional review board approved the use of MPT in TACE and written informed consent was obtained for each patient before the procedure. This was a retrospective study using imaging data and clinical records with no change in patient care. Institutional review board approval is not required at our institution for this type of study.

Patients

We defined superselective TACE as TACE performed at the more distal level of the subsegmental artery of the hepatic artery, including ultraselective TACE (TACE at the most distal level of the subsubsegmental artery) and subsegmental TACE (TACE at the subsegmental artery). Between October 2009 and October 2010, we treated 129 newly developed HCC lesions smaller than 6 cm in diameter in 87 patients (46 men and 41 women, mean age ± standard deviation, 73.0 ± 7.8 years; range 48–88 years) with superselective TACE. Tumor diameter ranged from 7 to 54 mm (18.4 ± 9.5 mm).

Diagnosis of HCC was established on the basis of findings from computed tomography (CT) imaging and/or magnetic resonance imaging (MRI)—characteristic homogenous or mosaic-like nodular enhancement on the arterial phase and wash out on delayed phase images, in addition to nodular staining on angiography and/or CT during hepatic arteriography (CTHA), and nodular perfusion defect on CT during arterial portography (CTAP) obtained using cone-beam CT (CBCT).

The patients were divided into three groups according to the type of anticancer drug used in the TACE procedure. Table 1 shows the patient characteristics for each group. Fifty-one tumors of 33 patients were treated with TACE using a mixture of iodized oil (Lipiodol; Andre Guerbet, Aulnaysous-Bois, France), contrast material (370 mg I/ml iopamidol, Iopamiron 370; Bayer Schering Pharma, Osaka, Japan), EPI, and M (EPI-M-TACE group). Twenty-one tumors of 15 patients were treated with TACE using an MPT-iodized oil suspension (miriplatin/LPD) (MPT-TACE group). Fifty-seven tumors of 39 patients were treated with TACE using a mixture of MPT/LPD and contrast material (MPT-I-TACE group). EPI-M-TACE was performed between October 2009 and April 2010, MPT-TACE was performed between January 2010 and June 2010, and MPT-I-TACE was performed between July 2010 and October 2010. Between January 2010 and April 2010, both EPI-M-TACE and MPT-TACE were performed. Selection of anticancer drugs was not randomized and was decided on the basis of the physician's preference.

TACE procedure

All TACE procedures were performed superselectively by use of a microcatheter with a tip less than 2F (Carnelian PIXIE; Tokai Medical Products, Kasugai, Japan; Progreat Σ; Terumo, Tokyo, Japan) through a 4F catheter. In the EPI-M-TACE group, 2–5 ml iodized oil, a contrast material of 1/3 iodized oil, and anticancer drugs (10–30 mg EPI and 2–6 mg M) were mixed by pumping 10 times by use of a three-way stopcock valve and two 5 to 10-ml syringes. In the MPT-TACE group, one vial of MPT (70 mg) was dissolved in 4 ml iodized oil (MPT/LPD). In the MPT-I-TACE group, a contrast material of 1/2 MPT/LPD was mixed in to create an emulsion by the same technique as described above. In both the MPT-TACE and MPT-I-TACE groups, the maximum dose of MPT was limited to 140 mg. The total amount of iodized oil was determined on the basis of the tumor size in each group. After injection of a mixture of iodized oil and anticancer drugs, gelatin sponge particles (Gelpart; Nippon Kayaku, Tokyo, Japan; approximately 0.5 or 0.2 mm in diameter), crushed by pumping 20 or 50 times by use of a three-way stopcock valve and two 2.5-ml syringes, were injected to completely obstruct the tumor-feeding branch in all three groups.

Table 1 Patient characteristics of each group

	EPI-M-TACE group	MPT-TACE group	MPT-I-TACE group
No. of patients	33	15	39
Male/female	16/17	6/9	24/15
Age	71.9 ± 7.9	75.3 ± 4.7	72.0 ± 8.5
Etiology (HCV/HBV/others)	22/5/6	11/4/0	24/7/8
Child–Pugh class (A/B/C)	16/12/5	12/3/0	24/14/1
T factor (T1/T2/T3)[a]	12/16/5	4/8/3	17/16/6
AFP level (ng/ml)	39.7 ± 57.7	445.8 ± 1856.2	238.5 ± 1100.9
PIVKA-II level (mAU/ml)	445.8 ± 1856.2	807.7 ± 1864.4	204.4 ± 506.9
No. of previous TACE sessions	1.4 ± 1.9	1.3 ± 1.8	1.7 ± 2.3

HCV hepatitis C virus, *HBV* hepatitis B virus, *AFP* alpha-fetoprotein, *PIVKA-II* protein induced in vitamin K absence II

[a] Definitions of TMN stage proposed by the Liver Cancer Study Group of Japan

Follow-up

Unenhanced CT was performed 1 week after TACE for all patients to check for iodized oil accumulation in the target tumor.

All patients were followed-up and dynamic CT and/or MRI were performed every 2–3 months after the TACE procedures to investigate tumor recurrence. Local recurrence was judged when an early enhancing tumor without iodized oil accumulation was observed in or adjacent to the tumor and/or confirmed by follow-up angiography, CBCTHA, and CBCTAP. Local recurrence was also classified into two patterns; intratumoral recurrence (IR) and peritumoral recurrence (PR) (Fig. 1) [4]. IR was defined as viable tumor correspondence to a defect in which iodized oil had previously been accumulated. PR was defined as a tumor adjacent to an iodized oil accumulated tumor without a defect.

Follow-up angiography and additional TACE for the recurrent tumor were performed if possible. The conditions of previously embolized branches were classified into three grades; reopened, attenuated, and occluded. Development of arterioportal shunts related to previous TACE was also evaluated.

Statistical analysis

Statistical comparison of patient age, tumor diameter, number of the embolized arterial branches, and duration of follow-up periods was performed by one-factor analysis of variance (ANOVA). If statistically significant differences among the three groups were observed, Tukey–Kramer tests were also performed. The gender, etiology of the chronic liver disease, Child–Pugh class, T-factor, TACE levels, IR, and incidence of occlusion or attenuation of the embolized branches of each group were compared by use of the χ^2 test. Incidence of cumulative local recurrence was calculated by use of the Kaplan–Meier method and compared. The generalized Wilcoxon test was used to evaluate significant differences in each group. Values of $P < 0.05$ were considered significant. Statistical calculations were performed by use of StatView version 5.0 software (SAS, Cary, NC, USA).

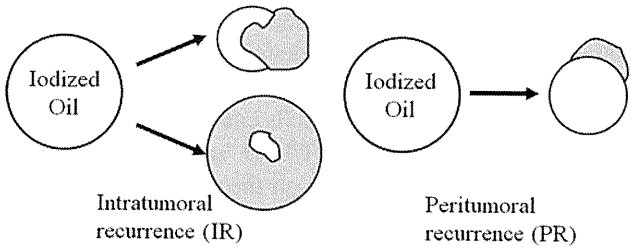

Fig. 1 Schematic representation of intratumoral and peritumoral recurrence. Intratumoral recurrence (*IR*) was defined as viable tumor correspondence to a defect in which iodized oil had previously been accumulated. Peritumoral recurrence (*PR*) was defined as a tumor adjacent to an iodized oil accumulated tumor without a defect

Results

Results are summarized in the Table 2.

Patient characteristics, tumor diameter, levels of TACE, number of embolized branches, and follow-up periods

There were no significant differences in gender, age, etiology of chronic liver disease, Child–Pugh class, and T-factor among the three groups ($P = 0.2970$, 0.3125, 0.4102, 0.0890, and 0.8346, respectively). There were also no significant differences in tumor diameter, levels of the TACE procedure, or number of the embolized arterial branches among the three groups ($P = 0.2857$, 0.8292, and 0.3157, respectively). The follow-up period for the EPI-M-TACE group was significantly longer than those for the MPT-TACE and MPT-I-TACE groups ($P < 0.01$ and 0.001, respectively). There was also a significant difference in the follow-up periods between the MPT-TACE and MPT-I-TACE groups ($P < 0.05$).

Local tumor recurrence

Dense iodized oil accumulation compared with the surrounding liver parenchyma was observed for all target

Table 2 Summary of each group

	EPI-M-TACE group	MPT-TACE group	MPT-I-TACE group
No. of tumors	51	21	57
Tumor diameter (mm)	16.9 ± 9.1	20.7 ± 11.3	18.8 ± 9.1
No. of embolized branches	1.8 ± 0.6	1.4 ± 0.7	1.6 ± 0.9
No. of subsegmental TACE (%)	7 (13.7)	4 (19.0)	8 (14.0)
Follow-up period (mo)	15.5 ± 4.7	12.0 ± 4.1	9.6 ± 3.1
Tumor recurrence (%)	13 (25.5)	14 (66.7)	31 (54.4)
Time to recurrence (mo)	9.6 ± 4.1	6.0 ± 3.4	5.2 ± 3.0
No. of IR (%)	3 (23.1)	10 (71.4)	22 (71.0)

IR intratumoral recurrence

tumors in each group on CT performed 1 week after TACE (Figs. 2, 3).

Local recurrence was observed in 13/51 tumors (25.5%) in the EPI-M-TACE group (Fig. 2), 14/21 tumors (66.7%) in the MPT-TACE group, and 31/57 tumors (54.4%) in the MPT-I-TACE group (Fig. 3). Four of 13 tumors (30.8%) in the EPI-M-TACE group, 4/14 tumors (28.6%) in the MPT-TACE group, and 5/21 tumors (23.8%) in the MPT-I-TACE group recurred after subsegmental TACE. Cumulative local recurrence in the EPI-M-TACE, MPT-TACE, and MPT-I-TACE groups after 5, 10, and 15 months was 6.1, 47.6, and 40.1%, 23.5, 67.3, and 63.9%, and 26.2, 75.4, and 72.9%, respectively. Local recurrence in the EPI-M-TACE group was significantly less than that in the MPT-TAE and MPT-I-TACE groups ($P < 0.0001$ and 0.0001, respectively) (Fig. 4).

Among recurrent tumors, IR in the EPI-M-TACE, MPT-TACE, and MPT-I-TACE groups was 23.1% (3/13), 71.4% (10/14), and 71.0% (22/31), respectively. IR in the EPI-M-TACE group was significantly lower than that in the MPT-TACE and MPT-I-TACE groups ($P < 0.05$ and 0.05, respectively).

Follow-up angiography findings

Follow-up angiography was performed for 11/13 recurrent tumors in the EPI-M-TACE group, 9/14 in the MPT-TACE group, and 28/31 in the MPT-I-TACE group. In the EPI-M-TACE group, the embolized branch was attenuated in eight tumors (72.7%). In three tumors (27.3%), the embolized branch was occluded and the neighboring hepatic branch or extrahepatic collateral vessel supplied the recurrent tumor (Fig. 2). In addition, arterioportal shunts in the previously embolized area developed in four tumors (36.4%) (Fig. 2). In the MPT-TACE group, all embolized branches were reopened. In the MPT-I-TACE group, the embolized branch was reopened in 19 tumors (67.9%) (Fig. 3) and attenuated in nine (32.1%). Occlusion or attenuation of the embolized branches in the EPI-M-TACE group was significantly higher than that in the MPT-TACE and MPT-I-TACE groups ($P < 0.001$ and 0.001, respectively). Arterioportal shunts were not observed in either the MPT-TACE group or the MPT-I-TACE group.

Discussion

TACE is an effective therapeutic options for inoperable HCC [1–4]. To enhance the therapeutic effect and reduce complications associated with TACE, superselective TACE using a microcatheter has become a standard TACE technique for small HCC throughout the world [2–4].

A single anticancer drug, or a combination of several, for example doxorubicin, EPI, M, and cisplatin, have been used in TACE; however, the importance of anticancer drugs in superselective TACE is still unknown. In randomized control studies, there was no evidence that TACE was more effective than transcatheter arterial embolization (TAE) [9, 10]. Kawai et al. [10] reported that the serum alpha-fetoprotein level decreased to a significantly greater extent in the group that received doxorubicin than in the group that did not, although survival was not significantly different between TAE with and without doxorubicin. This result suggested that doxorubicin had some favorable additional effect in TACE. Malagari et al. [11] reported that local recurrence after TACE using doxorubicin-loaded microspheres was significantly lower than after TAE using microspheres, although 1-year survival was no different between the two groups because of the short follow-up. They mentioned that the rationale for addition of a chemotherapeutic agent(s) in TACE is based on the assumption that chemotherapeutics augment the antitumoral action of ischemia, counteracting the stimulation of neoangiogenesis resulting from hypoxia due to embolization [11].

The most effective and least toxic regime in TACE has not yet been established. Several authors have reported that TACE using cisplatin resulted in better overall survival than TACE with doxorubicin or EPI [12–14]. However, cisplatin has severe side effects, including thrombocytopenia, hepatic failure, renal failure, and hypersensitivity reactions [15]. In addition, pre and post-hydration is required to prevent renal damage. MPT is a lipophilic platinum complex and 1,2-diaminocyclohexane platinum(II) dichloride, the active platinum compound binding to the nuclear DNA of tumor cells causing cytotoxicity, is gradually released from MPT/LPD accumulated in the tumor [5–8]. Therefore, MPT can theoretically reduce the adverse effects of platinum and does not require additional hydration. Okusaka et al. [7] reported good results with TAI using MPT/LPD for HCC, and recently it has also been used in TACE, because addition of embolic materials may result in more favorable antitumor effects than TAI [8].

In this study, local tumor recurrence was divided into two patterns; IR and PR [4]. IR may be indicative of incomplete TACE, for example insufficient blockage of the feeding artery or missing of other small feeding branches. PR may be indicative of residual minute tumor growth adjacent to the main mass, fed in part by the portal vein. Therefore, PR usually becomes apparent later than IR after TACE. After introduction of MPT into superselective TACE, we frequently experienced early local tumor recurrence, in particular IR. During the injection of MPT/LPD, the flow through tumor-feeding branches frequently